Inorganica Chimica Acta 370 (2011) 382–387

Contents lists available at ScienceDirect

Inorganica Chimica Acta

journal homepage: www.elsevier.com/locate/ica

Novel heterometallic palladium–silver complex

Natalia Yu. Kozitsyna [a,*], Sergei E. Nefedov [a], Alla P. Klyagina [a], Alexander A. Markov [a], Zhanna V. Dobrokhotova [a], Yuri A. Velikodny [b], Dmitry I. Kochubey [c], Tatiana S. Zyubina [d], Alexander E. Gekhman [a], Michael N. Vargaftik [a], Ilya I. Moiseev [a]

[a] N.S. Kurnakov Institute of General and Inorganic Chemistry, Russian Academy of Sciences, 119991 Moscow, Russian Federation
[b] M.V. Lomonosov Moscow State University, 119991 Moscow, Russian Federation
[c] G.K. Boreskov Institute of Catalysis, Siberian Branch of Russian Academy of Sciences, 630090 Novosibirsk, Russian Federation
[d] Institute for New Chemical Problems, Russian Academy of Sciences, 142432 Moscow Region, Chernogolovka, Russian Federation

ARTICLE INFO

Article history:
Received 22 December 2010
Received in revised form 28 January 2011
Accepted 1 February 2011
Available online 5 March 2011

Keywords:
Palladium
Silver
Heterometallic complexes
X-ray structure
Quantum-chemical analysis
Thermal decomposition

ABSTRACT

The reaction between $Pd_3(OOCMe)_6$ and $Ag_2(OOCMe)_2$ afforded the first palladium–silver heterometallic acetate-bridged complex $Pd^{II}[(\mu\text{-}OOCMe)_2Ag^{I}(HOOCMe)_2]_2$ (**1**). The molecular geometry and electronic structure of **1** were studied by single-crystal XRD and quantum-chemical DFT calculations. Thermal transformations of **1** *in vacuo* and under Ar, H_2 produced PdAg alloy nanoparticles characterized with powder XRD and EXAFS.

1. Introduction

Silver(I) acetate is still not clearly understood complex of this metal. Particularly, its XRD crystal structure was properly documented just recently [1]. Meanwhile, the transition and precious metal carboxylates become a challenge of current coordination chemistry [2–4]. Both monometallic and particularly heterometallic carboxylates are valuable precursors for molecular magnets [2,5], catalysts [6–9] and other nanostructural materials.

Recently we synthesised and structurally characterized the paddlewheel tetra(acetate)-bridged $Pd^{II}(\mu\text{-}OOCMe)_4Cu^{II}(OH_2)(HOOCMe)_2$ [10] and trinuclear palladium–copper bis(acetate)-bridged $Pd_2^{II}(\mu\text{-}OOCMe)_6Cu^{II}$ [11] complexes. In this work, using similar synthetic approach, we prepared the first acetate-bridged palladium–silver complex $Pd^{II}[(\mu\text{-}OOCMe)_2Ag^{I}(HOOCMe)_2]_2$ (**1**) and studied its structure and thermal transformations into Pd–Ag nanoparticles. A comparative quantum-chemical DFT study of complex **1**, its virtual formate (**1f**) and trifluoroacetate (**1tf**) analogs as well as the homonuclear silver(I) carboxylates $Ag_2(\mu\text{-}OOCR)_2$ (R = Me (**2**), H (**2f**) and CF_3 (**2tf**)) and hypothetical complex $Pd(\mu\text{-}OOCMe)_2Ag$ (**3**) revealed conditions for the metal–metal bonding in these molecular systems.

2. Results and discussion

2.1. Synthesis and structure

By analogy with the previous syntheses [10,11] we found that the reaction of $Pd_3(OOCMe)_6$ with $Ag_2(\mu\text{-}OOCMe)_2$ (**2**) in hot acetic acid produces the crystalline heterobimetallic complex $Pd^{II}[(\mu\text{-}OOCMe)_2Ag^{I}(HOOCMe)_2]_2$ (**1**, Fig. 1).

X-ray diffraction study showed that the Pd atom in molecule **1** is square-plane coordinated to four oxygen atoms of four bridging acetate ligands (Pd–O 2.0062(9)–2.0063(9) Å, Ag–O 2.3535(12), 2.3535(12) Å) (Table 1).

The $PdAg_2$ metal core of **1** is a linear metal chain (Ag–Pd–Ag angle is 180°), the Ag–Pd distances are fairly short (Pd···Ag 2.9194(2), 2.9195(2) Å). Slightly distorted tetrahedral coordination of each Ag atom is complemented with two terminal acetic acid ligands (Ag–O 2.4118(12), 2.4118(12) Å). The H atoms of the coordinated AcOH molecules are H-bonded to O atoms of the bridging acetate ligands of the adjacent molecules **1** (O···O 2.608(1) Å), forming in the crystal the linear polymer $\{Ag_2Pd(\mu\text{-}OOCMe)_4(HOOCMe)_4\}_n$ (Fig. 2) with close intermolecular Ag···Ag contacts 3.7641(2) Å and Ag···O 3.1102(9), 3.1102(9) Å).

Chemical reactivity studies showed that two-bridged molecule **1** is less chemically stable compared to the tetrabridged Pd complexes $Pd(OOCMe)_4ML_n$ (M = Ni^{II}, Co^{II}, Zn^{II} and Mn^{II}) with rather short metal–metal distances (2.55–2.65 Å) [11]. For example, the

* Corresponding author.
E-mail address: nkoz2009@gmail.com (N.Yu. Kozitsyna).

0020-1693/$ - see front matter © 2011 Elsevier B.V. All rights reserved.
doi:10.1016/j.ica.2011.02.003

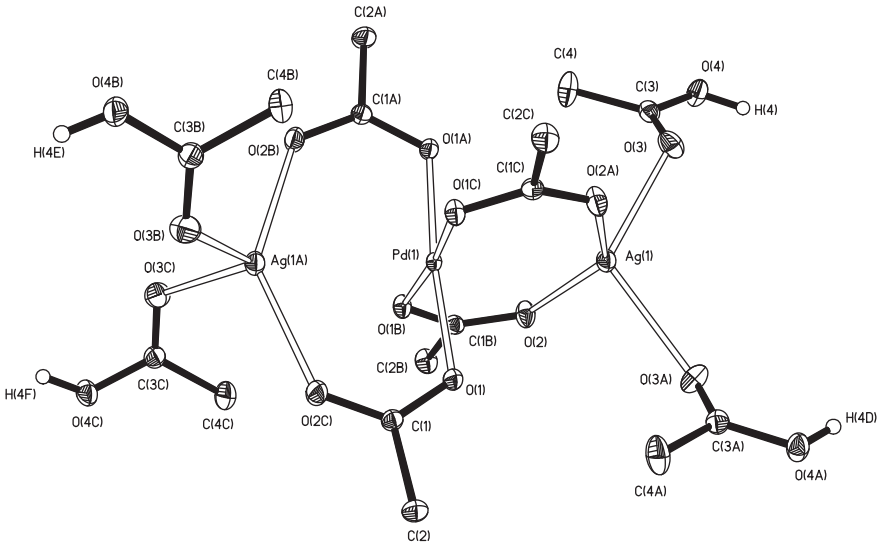

Fig. 1. Molecular structure of the formula unit of the complex $Pd^{II}[(\mu\text{-}OOCMe)_2Ag^{I}(HOOCMe)_2]_2$ (**1**) with thermal ellipsoids drawn at 50% probability level.

Table 1
Selected bond lengths (Å) and angles (°) for Complex **1**.

Bond lengths (Å)			
Ag(1)–Pd(1)	2.9195(2)	Pd(1)–Ag(1)#3	2.9194(2)
Pd(1)–O(1)	2.0063(9)	Pd(1)–O(1)#1	2.0063(9)
Pd(1)–O(1)#2	2.0062(9)	Pd(1)–O(1)#3	2.0063(9)
Ag(1)–O(2)	2.3535(12)	Ag(1)–O(2)#1	2.3535(12)
Ag(1)–O(3)	2.4118(12)	Ag(1)–O(3)#1	2.4118(12)
Bond angles (°)			
Ag(1)#3–Pd(1)–Ag(1)	180.0	O(1)–Pd(1)–Ag(1)	86.81(4)
O(1)#1–Pd(1)–Ag(1)	86.81(4)	O(1)#2–Pd(1)–Ag(1)	93.19(4)
O(1)#3–Pd(1)–Ag(1)	93.19(4)	O(1)–Pd(1)–Ag(1)#3	93.19(4)
O(1)#1–Pd(1)–Ag(1)#3	93.19(4)	O(1)#2–Pd(1)–Ag(1)#3	86.81(4)
O(1)#3–Pd(1)–Ag(1)#3	86.81(4)	O(2)–Ag(1)–Pd(1)	69.84(3)
O(2)#1–Ag(1)–Pd(1)	69.84(3)	O(3)–Ag(1)–Pd(1)	123.56(3)
O(3)#1–Ag(1)–Pd(1)	123.56(3)	O(1)–Pd(1)–O(1)#1	173.62(9)
O(1)#2–Pd(1)–O(1)	90.179(5)	O(1)#2–Pd(1)–O(1)#3	173.62(9)
O(1)–Pd(1)–O(1)#3	90.178(5)	O(1)#2–Pd(1)–O(1)#1	90.177(5)
O(1)#3–Pd(1)–O(1)#1	90.176(5)	O(2)–Ag(1)–O(3)	108.80(4)
O(2)–Ag(1)–O(3)#1	93.37(4)	O(2)#1–Ag(1)–O(2)	139.68(6)
O(2)#1–Ag(1)–O(3)	93.37(4)	O(2)#1–Ag(1)–O(3)#1	108.80(4)
O(3)–Ag(1)–O(3)#1	112.88(7)		

Symmetry transformations used to generate equivalent atoms: #1 $-x,-y,z$ #2 $-y,x,-z$ #3 $y,-x,-z$.

reaction of the latter complexes with Phen and pivalic acid does not violate the acetate-bridged heterometallic core [12a,b]. Unlike this, complex **1** is decomposed by Phen or PivH into the monometallic Ag carboxylates and complexes $PhenPd(OOCMe)_2$ or $Pd(OOCBu^t)_2$, respectively.

Nevertheless, the relatively short Ag–M distance in molecules **1** (2.919 Å, M = Pd) and **2** (2.852 Å, M = Ag) could suggest some metal–metal bonding. For instance, direct Ag–Ag bonding was recently proposed [1] on the basis of Bader's AIM analysis of molecule **2** and the band at 80–85 cm^{-1} found in its Raman spectrum. The bond order of 0.2 in the fluorinated silver(I) acetates was calculated in works [15a,b]. Meanwhile, the Ag–Ag bond was not found in the $Ag_2(NO_3)_2$ fragment of the supramolecular silver(I) complex with *trans*-1,2-bis(4-piridyl)ethylene [16]. Hence, it was of interest to analyze the electron interaction in molecules **1** and **2**.

2.2. Quantum chemical analysis of *1* and *2*

The well known Cotton scheme of "metallic" MOs [14a–c] suggests the absence of the direct M–M′ bonding in binuclear late transition metal complexes. Meanwhile, the possibility of bonding M–M′ interactions in polynuclear late metal compounds is now argued [1,13a,b,14c,15a,b].

In this work we carried out a DFT study of the electronic structure and chemical bonding in molecules **1** and **2**, as well as in the formate (**1f** and **2f**) and trifluoroacetate analogs (**1tf**, **2tf**) and hypothetical complex $Pd(\mu\text{-}OOCMe)_2Ag$ (**3**) with B3LYP functional [17a,b] using the CEP-121G basis set and GAUSSIAN 03 program [18].

The geometry optimization for complexes **1** and **2** gave quite reasonable agreement between the calculated and experimental values (Tables 2 and 3).

As seen in Tables 2 and 3, the singlet states are much more favorable than the triplet ones for all the complexes. The calculated geometry of **1** and **2** well agree with experimental data for the singlet states. The interatomic distances D(Pd–Ag) in **1** and D(Ag–Ag) in **2** and their analogs are shortened upon excitation to the triplet state, which can be an indication on M–M′ bonding in this state, whereas the bonding is absent in the singlet state. This is in agreement with the antibonding character of the HOMO in **1** and **2** and nonbonding and bonding character of LUMO in **1** (Fig. 3) and **2**, respectively (see Fig. 6 in [1] for **2**; similar frontal MOs were found in our calculations). The overlap populations P(Ag–Ag) data in Table 3 confirm these conclusions.

NBO analysis showed that complexes **2** have no bonding natural orbitals (NO) in the M–M′ fragment in singlet state, whereas the triplet state has a bonding NO in α-representation, providing a bond order of 0.5. Similar trends in geometric and electronic structure were found for complexes **2f** and **2tf**.

The heterometallic complex **3** is isoelectronic to cation $\mathbf{2}^{+}$, which contains only one electron at the antibonding MO. This fact can be responsible for shorter interatomic distances D(Ag–Ag) in $\mathbf{2}^{+}$ and D(Pd–Ag) in **3** compared to D(Ag–Ag) in **2** (Table 2). The HOMO in α- and LUMO in β-representation for **3** have the same antibonding character as the HOMO in **2**. Taking into account these results together with the overlap populations P(Pd–Ag), we can suggest some Pd–Ag bonding in the B doublet ground state of **3**(D) and its further increase on going to $\mathbf{3}^{+}$ and quartet state of **3**(Q) (Table 3).

A change in D(Pd–Ag) (Table 2) observed in the cation $\mathbf{1}^{+}$ and triplet state of molecule **1** well agree with the expected effect of

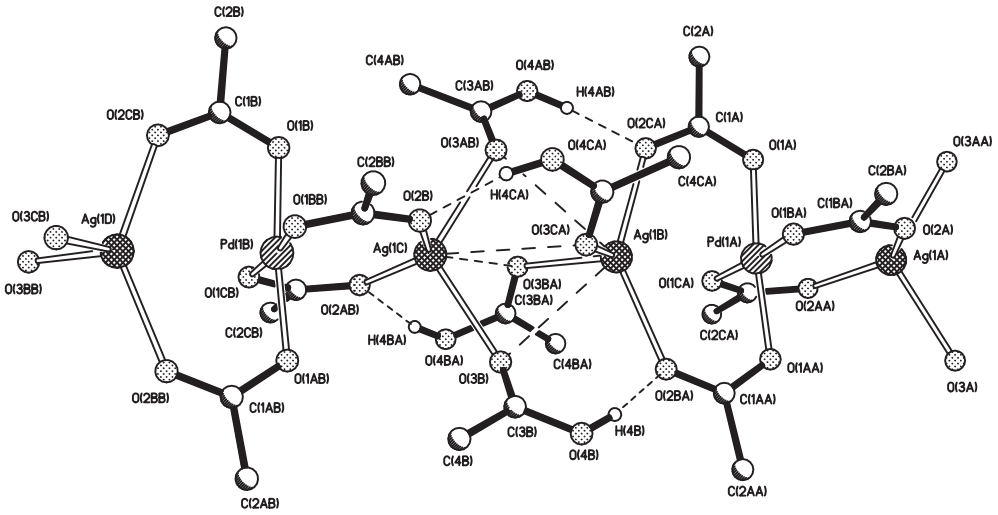

Fig. 2. Fragment of the polymer chain $\{Pd^{II}[(\mu\text{-}OOCMe)_2Ag^{I}(HOOCMe)_2]_2\}_n$ of **1** in the crystal.

Table 2
Interatomic distances (D, Å) in the complexes $Pd^{II}[(\mu\text{-}OOCX)_2Ag^{I}(HOOCX)_2]_2$ (**1**, **1**$^+$, **1**$^-$ and **1f**) and the energy differences ($\Delta E_{(S-T)}$, kcal/mol) between the singlet and triplet states calculated by DFT (B3LYP) with CEP-121G basis.

Complex	D(Pd–Ag)	D(Pd–O)	D(Ag–O)	D(Ag–O′)	$\Delta E_{(S-T)}$
1, X = CH_3, S	2.991	2.061	2.338	2.462	−23.6
1, X = CH_3, T	2.740	2.217	2.206	2.513	
Experiment	2.919	2.006	2.354	2.412	
1$^+$ *cation*, X = CH_3, D	2.736	2.035	2.225	2.435	
1$^-$ *anion*, X = CH_3	2.931	2.256	2.331	2.599	
1f, X = H, S	3.076	2.060	2.360	2.450	−38.9
1f, X = H, T	3.058	2.169	2.332	2.466	
1f$^+$ *cation*, X = H, D	2.750	2.037	2.236	2.424	
1f$^-$ *anion*, X = H	2.895	2.283	2.240	2.786	

Table 3
Interatomic distances (D, Å), overlap populations P(Ag–Ag) in the complexes $Ag_2(OOCX)_2$ and the energy differences ($\Delta E_{(S-T)}$, kcal/mol) between the singlet and triplet states calculated by DFT (B3LYP) with CEP-121G basis.

Complex	D(Ag–Ag)	P(Ag–Ag)	D(Ag–O)	P(Ag–O)	$\Delta E_{(S-T)}$
2, X = CH_3, S	2.852	0.003	2.146	0.128	−77.1
2, X = CH_3, T	2.741	0.116	2.168	0.123	
Experiment[a]	2.803		2.200		
2$^+$, *cation*, X = CH_3, D	2.655	0.058	2.101	0.140	
2$^-$, *anion*, X = CH_3, D	2.977	0.078	2.142	0.138	
2f, X = H, S	2.876	0.020	2.153	0.127	−81.1
2f, X = H, T	2.736	0.131	2.176	0.122	
2tf, X = CF_3, S	2.962	0.014	2.161	0.111	−84.5
2tf, X = CF_3, T	2.732	0.132	2.191	0.123	
Experiment[b]	2.967		2.232		
	D(Pd–Ag)	P(Pd–Ag)			$\Delta E_{(D-Q)}$
3, X = CH_3, D	2.730	0.009	2.142	0.132	−72.5
3, X = CH_3, Q	2.659	0.129	2.401	0.073	
3$^+$, X = CH_3	2.593	0.066	2.105	0.141	

[a] Ref. [1].
[b] Ref. [18].

electron removal from the strongly antibonding HOMO (Table 2). On going to anion **1**$^-$, the addition of electron to the nonbonding LUMO results in minor variation of D(Pd–Ag). Interestingly that the terminal HO–(COMe) groups in the optimized geometry of anion **1**$^-$ are noticeably approached to the O atoms of bridging MeCOO groups compared to those in **1** (Fig. 4) and **1**$^+$, whereas the O–H bonds lengthen from 0.985 Å in **1** (s and t) and **1**$^+$ to 1.06 Å in **1**$^-$ and the distance between H and O in CH_3COO group is 1.43 Å.

In the case of formate complex **1f**$^-$ no change in the geometry was found. The OH groups in the coordinated HCOOH molecules are arranged in the same way as in **1f** (s and t) and **1f**$^+$, and the O–H bond length is 0.986 Å in all the formate species. The rest trends in the electronic state and geometry in the series **1f**(s) **1f**(t), **1f**$^+$ and **1f**$^-$ are the same as those in the acetate analogs (Table 2).

Hence, we can draw a conclusion that molecules **1** and **2** in the singlet ground states have no Ag–M (M = Pd, Ag) direct electron interaction, whereas excitation to the triplet (**1**T, **1f**T, **2**T, **2f**T and **2tf**T) states gives rise to the metal–metal bonding.

2.3. Thermal transformations of *1*

2.3.1. Thermolysis in inert atmosphere

Thermal transformations of complex **1** under Ar occur in two clear-cut stages (Fig. 5). The first stage, in the interval 75.5–117 °C (±1.5 °C), is accompanied with a mass loss of 29.1 ± 1.0 % and a strong composite endotherm of 224.8 ± 5.5 kJ/mol (including three close overlapping endotherms with maxima at 92.4, 101.4 and 109.7 °C). The found mass loss is close to the calculated value for complete removal of four coordinated acetic acid molecules (30.08%).

Since the intermediate formed at the first stage does not change during further heating within 117–150 °C, it would seem that the removal of the coordinated acetic acid ligands produced a new, sufficiently stable metal complex. However, XRD analysis showed that the intermediate product (prepared in separate experiment by heating to 120 °C with a rate of 10°/min followed by fast quenching under Ar) consists of several distinctive phases, Pd(II) and Ag(I) acetates and small admixtures with unidentified XRD peaks. IR spectrum of the intermediate product revealed only bridging acetate groups. Hence, the intermediate Pd–Ag complex, if formed, easily decomposes into monometallic components.

The second stage of thermolysis (150–260 °C) is accompanied with a weight loss of 28.9 ± 1.0% and a small exotherm (Fig. 5). Total weight loss in two stages is 58.0% (±1.0%). XRD analysis showed that the final solid product is a mixture of the PdO, Ag and PdAg alloy phases. The formation of PdO and Ag is in agreement with known data on the thermolysis of Pd(II) acetate [19a] and Ag(I) acetate [19b], respectively. The PdAg alloy seems to form from an unstable heterometallic intermediate. In a separate experiment, when thermolysis process was driven to 450 °C, our XRD data revealed two different PdAg phases in the final product.

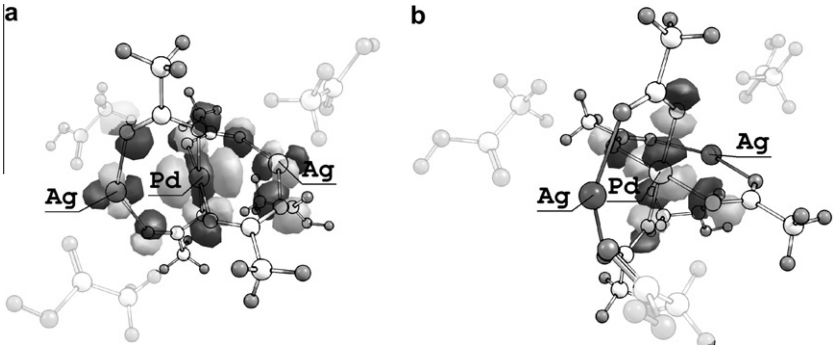

Fig. 3. HOMO (a) and LUMO (b) of molecule **1**.

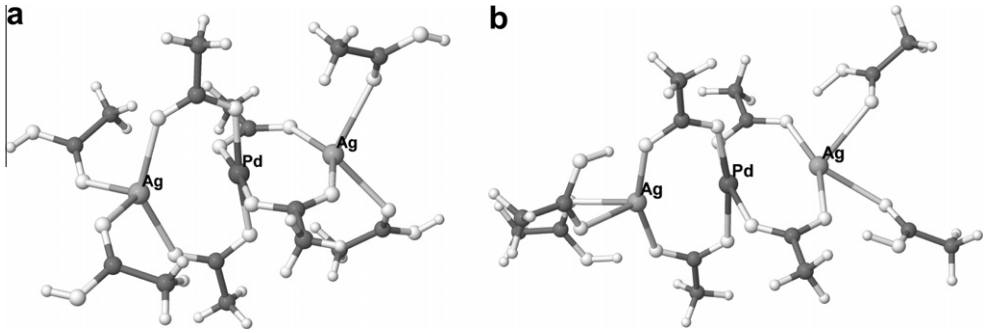

Fig. 4. Optimized geometry of the molecule **1** (a) and anion $\mathbf{1}^-$ (b).

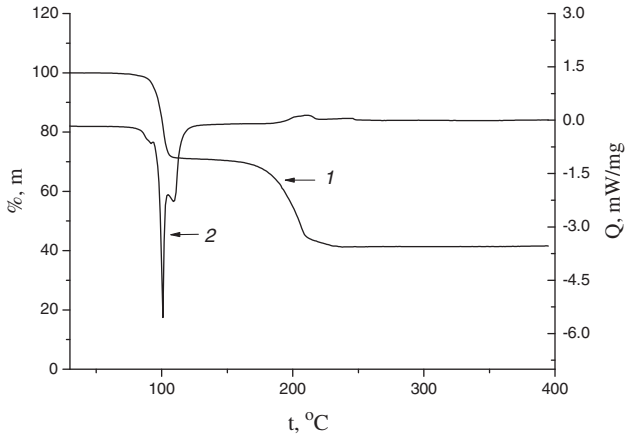

Fig. 5. TGA–DSC data for thermal decomposition of **1** (Ar flow, heating rate 10 deg/min): *1* – TGA curve; *2* – DSC curve.

2.3.2. Thermolysis in vacuo

When complex **1** was heated *in vacuo* to 500 °C, the reaction product was found by powder XRD to consist of PdAg alloy nanoparticles with a small admixture (~5%) of Ag nanophase. The crystallite sizes of PdAg and Ag were estimated by the Scherrer formula $\beta = K\lambda/L\cos\theta$, where β is the integrated peak width, K is the shape factor, λ is the wavelength and L is the volume (corrected for the instrumental broadening). The average crystallite size is 13 ± 2 and 67 ± 5 nm for PdAg and for Ag, respectively. Mass spectral analysis of the volatile reaction products revealed CO_2, CO, acetic acid, CH_4 and no acetone.

2.3.3. Thermolysis under H_2

Reduction of **1** with H_2 (1 atm of 10%H_2/90%He) at 250 °C produced a three-phase solid, which according to power XRD consists of the PdAg alloy (a = 4.0100(24) Å), Pd metal ($a \sim 3.91$ Å) and Ag metal (a = 4.079 Å) nanoparticles. The mean sizes of the crystallites estimated by the Scherrer formula are 13 nm for PdAg and 67 nm for Ag.

The EXAFS study (Fig. 6) revealed the main observable product of **1** reduction with H_2 at 300 °C as a PdAg alloy with the shortest metal–metal distance 2.82 Å, but with smaller ($\leqslant$5 nm) particle mean size. The inconsistency in the particle size estimates is most likely due to the fact that XRD is mainly sensitive to particles with mean size >5 nm, while a substantial fraction of the alloy particles seems to be smaller in size.

It is known that the palladium–silver solid alloy system is continuous and has no singularities or intermetallides [20]. Hence, different PdAg alloys could form depending on the experimental conditions. We estimated the composition of the solid PdAg alloys obtained in the above experiments, using the known empirical dependence [21a,b] for the Ag_xPd_{1-x} solid alloys:

$$a(x), a = 3.88635 + 0.1959x.$$

The H_2-reduced product turned to be a single-phase alloy of the composition $Ag_{0.63}Pd_{0.37}$. The product of **1** thermolysis under Ar at 450 °C consists of two phases: $Ag_{0.75}Pd_{0.25}$ and $Ag_{0.65}Pd_{0.35}$.

3. Experimental

3.1. Reagents and physical measurements

3.1.1. Reagents and solvents

Silver(I) acetate AgOOCMe, pivalic acid and solvents (acetic acid, benzene, acetonitrile and THF), all reagent grade were purchased from Acros Organics and used as received. Palladium(II) acetate $Pd_3(OOCMe)_6$ was prepared from $PdCl_2$ (Reakhim, Russia) by reduction with $NaBH_4$ followed by the oxidation of the Pd black with concentrated HNO_3 in glacial acetic acid according to a

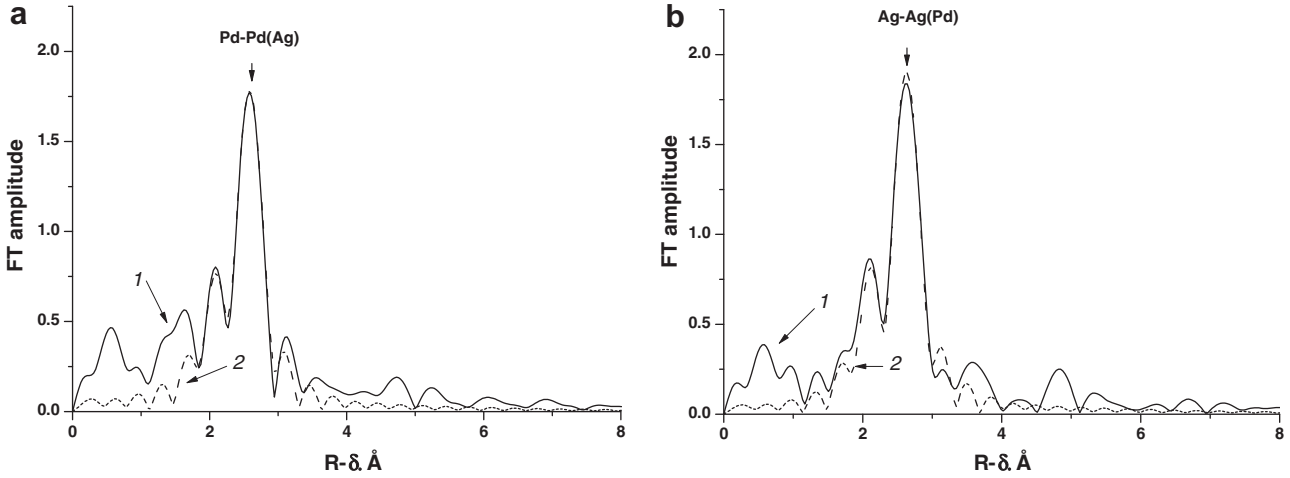

Fig. 6. Radial distribution function obtained from EXAFS data for the product of **1** reduction with H_2 at 300 °C: (a) Pd*K* edge, (b) Ag*K* edge; *1* – Fourier transform modulus; *2* – model for PdAg alloy.

procedure [22] and purified by repetitive recrystallisation from hot acetic acid.

3.1.2. Physical measurements

The elemental C,H,N analysis was performed on an automated C,H,N-analyzer (Carlo Erba Strumentazione, Italy). The IR spectra were recorded on a Nicolet Nexus spectrometer with a Pike micro-ATR accessory.

Thermoanalytic measurements were carried out on *NETZSCH TG 209 F1* and *NETZSCH DSC 204 F1* instruments in an Ar flow (20 ml/min) (Ar, >99.998%; O_2, 0.0002%; N_2, <0.001%; water vapor, <0.0003%; CH_4, <0.0001%). Samples were weighted on a *SARTORIUS RESEARCH R 160P* analytical balance with an accuracy of 1×10^{-2} mg. The calorimeter was calibrated by an ISO 11357-1 standard.

The thermal decomposition of **1** was studied by differential scanning calorimetry (DSC) and thermogravimetry (TGA). The thermogravimetric measurements were performed in alundum crucibles at a heating rate of 10 °C/min. The composition of the gas phase was studied on a QMS 403C Aëolos mass-spectrometric unit under TGA conditions. The ionizing electron energy was 70 eV; the highest determined mass number (mass-to-charge ratio) was 300 amu. The weight of the samples was 0.5–3 mg. The DSC study was carried out in aluminum cells at a heating rate of 10 °C/min. The weight of samples was 4–10 mg. Each experiment was repeated at least three times. The TGA–DSC data were processed by the ISO 11357-1, ISO 11357-2, ISO 11358, ASTM E 1269-95 standards with the use of the NETZSCH Proteus Thermal Analysis program package.

The X-ray powder diffraction analysis of the solid decomposition products was carried out on a G670 (HUBER) Guinier camera using $CuK_{\alpha 1}$ radiation and on an FR-552 monochromator chamber ($CuK_{\alpha 1}$ radiation) using germanium as the internal standard (X-ray diffraction patterns were processed on an IZA-2 comparator with an accuracy of ±0.01 mm).

The volatile products of **1** decomposition were detected by GC/MS on an Agilent 6890 Gas Chromatograph equipped with an Agilent 5973 mass-selective detector and 0.2 mm × 25 m capillary column.

3.2. X-ray diffraction analysis

Single-crystal X-ray diffraction experiments were carried out on a Bruker SMART APEX II diffractometer with a CCD area detector (graphite monochromator, Mo Kα radiation, $\lambda = 0.71073$ Å, ω-scans, $2\theta_{max} = 60°$). For complex **2**: $C_{16}H_{28}Ag_2O_{16}Pd$, $M = 798.52$, tetragonal, space group I-4, $a = b = 11.4895(7)$ Å, $c = 9.5453(7)$ Å, $V = 1260.06(14)$ Å^3 (100 K), $Z = 2$, $D_{calc} = 2.105$ g/cm^3, 5962 measured reflections, 1625 independent reflections with $F^2 > 2\sigma(I)$, $\mu = 2.318$ cm^{-1}, $R_1 = 0.0114$,, $wR_2 = 0.0285$. The semi-empirical method SADABS [23] was applied for the absorption correction. The structures were solved by direct methods and refined by the full-matrix least-squares technique against F^2 with the anisotropic displacement parameters for all nonhydrogen atoms. All the hydrogen atoms in the complexes were placed geometrically and included in the structure factors calculation in the riding motion approximation. All the data reduction and further calculations were performed using the SAINT [24] and SHELXTL-97 [25] program packages.

3.3. Synthesis and reactions

3.3.1. Pd[(μ-OOCMe)$_2$Ag(HOOCMe)$_2$]$_2$ (**1**)

A slurry of $Pd_3(OCOMe)_6$ (400 mg, 1.78 mmol based on Pd) and $Ag_2(OCOMe)_2$ (400 mg, 2.4 mmol based on Ag) in 35 ml of glacial acetic acid was stirred in a shadowed flask at 100 °C for 2 h. The reaction mixture was cooled ~50 °C and filtered from a dark-gray solid (unreacted and partially decomposed silver acetate). The mother liquid was stayed for 12 h in the dark at room temperature to produce a dark-yellow crystalline precipitate of **1** (277 mg). To the filtered mother liquid was added a new portion of **1** (300 mg, 1.8 mmol) followed by stirring at 100 °C for 2 h. Cooling and filtration gave an additional amount of **1** (201 mg). Then the third portion of $Ag_2(OCOMe)_2$ (200 mg, 1.2 mmol) was added to the mother liquid to afford additional amount of **1** (176 mg). Finally, the mother liquid was concentrated to the half of volume and gave a new portion of **1** (50 mg). Total yield of **1** was 704 mg (50% based on Pd). Complex **1** is soluble in acetic acid and water, insoluble in benzene and slightly soluble with fast decomposition in $CHCl_3$, CH_3CN, acetone and THF; it should be stored in the dark. *Anal.* Calc. for $PdAg_2C_{16}O_{16}H_{28}$: C, 24.07; H, 3.53. Found: C, 24.03; H, 3.48%. IR spectrum (ATR, ν/cm^{-1}): 1684s, 1603w, 1521vs, 1399vs,br, 1368w, 1374w, 1273s, 1016m, 946w, 890m, 696s, 673w, 619m.

3.3.2. Intermediate product of **1** thermolysis

Complex **1** (100 mg, 0.13 mmol) was heated in Ar flow (20 ml/min) to 120 °C with a rate of 5 °C/min and the residue was cooled under Ar to give 79.9 mg of the thermolysis product whose weight

corresponds to the loss of four molecules of acetic acid. *Anal.* Calc. for $PdAg_2C_8O_8H_{12}$: C, 17.26; H, 2.11. Found: C, 17.21; H, 2.17%. IR spectrum (ATR, ν/cm^{-1}): 1602m, 1558w, 1518vs, 11435w, 1396vs, 1345w, 1033m, 931w, 695m, 672s, 618m.

*3.3.3. Reaction of **1** with 1,10-phenanthroline*

A solution of Phen·H_2O (12.5 mg, 0.06 mmol) in 1 ml of benzene was added rapidly under stirring to a suspension of **1** (50 mg, 0.06 mmol based on Pd) in 1 ml of benzene. The reaction mixture was stirred at room temperature for 0.5 h until the initial complexes **1** completely dissolved. White floccular precipitate of Ag acetate was removed by filtration, washed with heptane and dried. *Anal.* Calc. for $AgC_2O_2H_3$: C, 14.39; H, 1.81. Found C, 14.63; H, 1.93%. Yield 12.6 mg (62%).The mother liquor was concentrated on a rotary evaporator to 1 ml and the pale-yellow Phen-$Pd(OCOMe)_2$ was precipitated by heptane (2 ml) and dried. The yield of $PhenPd(OCOMe)_2$ was 19 mg (75% based on Pd). *Anal.* Calc. for $PdC_{16}O_4N_2H_{14}$: C, 47.48; N, 6.92; H, 3.49. Found C, 47.51; N, 7.04; H, 3.53%. IR spectrum (KBr, cm^{-1}): 2956w, 2926w, 2869w, 1601s, 1480m, 1400m, 1354m, 1221m, 848w, 7784w, 715w, 644w.

*3.3.4. Reaction of **1** with pivalic acid*

A solution of pivalic acid (51.1 mg, 0.5 mmol) in 1 ml of benzene was added under stirring to a suspension of **1** (100 mg, 0.125 mmol based on Pd) in 3 ml of benzene. The reaction mixture was stirred at room temperature for 1.5 h until the initial complex **1** completely dissolved. White floccular precipitate of Ag acetate was removed by filtration, washed with heptane and dried. *Anal.* Calc. for $AgC_2O_2H_3$: C, 14.39; H, 1.81. Found C, 15.08; H, 2.01%. Yield 30.4 mg (73%). The mother liquor was concentrated on a rotary evaporator to 0.3 ml and stored for crystallization at room temperature for 12 h. The red-brown crystals of $Pd(OOCBu^t)_2$ were separated by decantation and dried. The yield of the crystalline complex was 24 mg (70% based on Pd). *Anal.* Calc. for $PdC_8O_4H_{18}$: C, 33.80; H, 6.39. Found C, 33.91; H 6.44%. IR spectrum (KBr, cm^{-1}): 2962m, 2929w, 1596s, 1556w, 1482m, 1456w, 1415s, 1378m, 1362w, 1225s, 780w, 633m.

4. Conclusion

In this work we prepared and X-ray structurally characterized the first heterometallic palladium(II)–silver(I) carboxylate complex $Pd^{II}[(\mu\text{-}OOCMe)_2Ag^{I}(HOOCMe)_2]_2$ (**1**). Quantum-chemical DFT and NBO analysis showed that molecule **1** and silver(I) acetate **2** have no Ag–M (M = Pd, Ag) direct electron interaction in the singlet ground states, whereas excitation to the triplet states can give rise to the metal–metal bonding. Chemical reactivity studies showed that unlike the known stable Pd^{II}-based tetra(carboxylate)-bridged paddlewheel heterometallics $Pd^{II}(\mu\text{-}OOCR)_4M^{II}(L)$ with divalent 3d-transition metals [10–12], the two-bridged Pd–Ag acetate **1** is sufficiently stable in the crystalline state up to 75 °C only and decomposes in solution or upon heating in inert atmosphere. Meanwhile, the easily prepared complex **1** can be a useful source for the preparation of Pd–Ag alloys under fairly mild conditions.

Acknowledgements

We thank for financial support the Russian Foundation for Basic Research (projects Nos. 09-03-00514, 09-03-12114, 10-03-90420 and 11-03-01157), the Foundation of President of the Russian Federation (program for support of leading Russian scientific schools NSh-65264.2010.3) and the Foundation of the Russian Academy of Sciences (programs for Basic Research "Purposeful synthesis of inorganic substances and creation of related functional materials" and "Theoretical and experimental investigation of the nature of chemical bonding and mechanisms of important reactions and processes").

Appendix A. Supplementary material

CCDC 802579 contains the supplementary crystallographic data for this paper. These data can be obtained free of charge from The Cambridge Crystallographic Data Centre via www.ccdc.cam.ac.uk/data_request/cif. Supplementary data associated with this article can be found, in the online version, at doi:10.1016/j.ica.2011.02.003.

References

[1] L.P. Olson, D.R. Whitcomb, M. Rajeswaran, T.N. Blanton, B.J. Stwertka, Chem. Mater. 18 (2006) 1667.
[2] (a) J.T. Brockman, K.A. Abboud, D.N. Hendrickson, G. Christou, Polyhedron 22 (2003) 1765;
(b) I.L. Eremenko, A.A. Sidorov, M.A. Kiskin, in: S.P. Gubin (Ed.), Magnetic Nanoparticles, Wiley, 2009, p. 349;
(c) M.H. Zeng, Y.L. Zhou, M.C. Wu, H.L. Sun, M. Du, Inorg. Chem. 49 (2010) 6436.
[3] G.I. Dzhardimalieva, A.D. Pomogailo, Russ. Chem. Rev. 77 (2008) 259.
[4] D.J. Tranchemontagne, J.L. Mendoza-Cortés, M. O'Keeffe, O.M. Yaghi, Chem. Soc. Rev. 38 (2009) 1257.
[5] E. Terazzi, C. Bourgogne, R. Welter, J.-L. Gallani, D. Guillon, G. Rogez, B. Donnio, Angew. Chem., Int. Ed. 47 (2008) 490.
[6] O.P. Tkachenko, A.Yu. Stakheev, L.M. Kustov, I.V. Mashkovsky, M. van den Berg, W. Grünert, N.Yu. Kozitsyna, Zh.V. Dobrokhotova, V.I. Zhilov, S.E. Nefedov, M.N. Vargaftik, I.I. Moiseev, Catal. Lett. 112 (2006) 155.
[7] L. Aschwanden, T. Mallat, J.-D. Grunwald, F. Krumeich, A. Baiker, J. Mol. Catal. 300 (2009) 111.
[8] Quing-An Chen, Wei Zeng, Da-Wei Wang, Yong-Gui Zhou, Synlett (2009) 2236.
[9] R. Gawin, K. Grela, in: Green Metathesis Chemistry (NATO Science for Peace and Security Series A: Chemistry and Biology), Springer, 2010, p. 57.
[10] N.S. Akhmadullina, N.V. Cherkashina, N.Yu. Kozitsyna, I.P. Stolarov, E.V. Perova, A.E. Gekhman, S.E. Nefedov, M.N. Vargaftik, I.I. Moiseev, Inorg. Chim. Acta 362 (2009) 1943.
[11] N.Yu. Kozitsyna, S.E. Nefedov, F.M. Dolgushin, N.V. Cherkashina, M.N. Vargaftik, I.I. Moiseev, Inorg. Chim. Acta 359 (2006) 2072.
[12] (a) S.E. Nefedov, M.N. Vargaftik, I.I. Moiseev, Inorg. Chim. Commun. 9 (2006) 755;
(b) N.Yu. Kozitsyna, S.E. Nefedov, Zh.V. Dobrokhotova, V.N. Ikorskii, I.P. Stolyarov, M.N. Vargaftik, I.I. Moiseev, Nanotechnol. Russ. 3 (2008) 166.
[13] (a) R. Alvarez, A.R. de Lera, J.M. Aurrecoechea, A. Durana, Organometallics 26 (2007) 2799;
(b) A.A. Markov, A.P. Klyagina, S.P. Dolin, N.S. Ahmadullina, N.Yu. Kozitsyna, N.V. Cherkashina, S.E. Nefedov, M.N. Vargaftik, I.I. Moiseev, Russ. J. Inorg. Chem. 54 (2009) 885.
[14] (a) F.A. Cotton, N.F. Curtis, C.B. Harris, B.F.G. Johnson, S.J. Lippard, J.T. Mague, W.R. Robinson, J.S. Wood, Science 145 (1964) 1305;
(b)F.A. Cotton, C.F. Murillo, R.A. Walton (Eds.), Multiple Bonds between Metal Atoms, third ed., Springer Science and Business Media, Inc., New York, 2005;
(c) J.F. Berry, E. Bill, E. Bothe, F.A. Cotton, N.S. Dalal, S.A. Ibragimov, N. Kaur, C.Y. Liu, C.A. Murillo, S. Nellutla, J.M. North, D. Villagran, J. Am. Chem. Soc. 129 (2007) 1393.
[15] (a) Yu.I. Tarasov, Z.G. Bazhanova, D.M. Kovtun, A.I. Boltalin, B.K. Novosadov, I.V. Kochikov, J. Struct. Chem. 49 (2008) 207;
(b) Z.G. Bazhanova, Yu.I. Tarasov, D.M. Kovtun, A.I. Boltalin, B.K. Novosadov, I.V. Kochikov, J. Struct. Chem. 51 (2010) 409.
[16] T.S. Zyubina, V. Razumov, S.B. Brichkin, V. Anisimov, S.H. Lin, A. Mebel, Russ. J. Inorg. Chem. 51 (2006) 885. 925.
[17] (a) A.D. Becke, J. Chem. Phys. 98 (1993) 5648;
(b) P.J. Stephens, F.J. Devlin, C.F. Chabalowski, M.J. Frisch, J. Phys. Chem. 98 (1994) 11623.
[18] M.J. Frisch, G.W. Trucks, H.B. Schlegel, et al., Gaussian 03. Revision C.02, Gaussian, Inc., Wallingford CT, 2004.
[19] (a) P.K. Gallagher, M.E. Gross, J. Therm. Anal. 31 (1986) 1231;
(b) V. Logvinenko, O. Polunina, Yu. Vikhilov, B. Bokhonov, J. Therm. Anal. Calorimetry 90 (2007) 813.
[20] I. Karakaya, W.T. Tompson, Bull. Alloy Phase Diagrams 9 (1988) 237. 289.
[21] (a) K. Baba, U. Miyagawa, K. Watanabe, Y. Sakamoto, T.B. Flanagan, J. Mater. Sci. 25 (1990) 3910;
(b) Y.C. Venudhar, L. Iyengar, K.V. Krishna Rao, J. Less-Common Metals 58 (1978) P55.
[22] T.A. Stephenson, S.M. Morehouse, A.R. Powell, J.P. Heffer, G. Wilkinson, J. Chem. Soc. (1965) 3632.
[23] G.M. Sheldrick, SADABS, Bruker AXS Inc., Madison, WI-53719, 1997.
[24] SMART V5.051 and SAINT V5.00, Area Detector Control and Integration Software, 1998, Bruker AXS Inc., Madison, WI-53719, USA.
[25] G.M. Sheldrick, SHELXTL-97 V5.10, Bruker AXS Inc., Madison, WI-53719, USA, 1997.